Perineuronal Nets, Inhibitory Interneurons and Anxiety-Related Ventral Hippocampal Neuronal Oscillations Are Altered by Early Life Adversity

Supplemental Information

Supplemental Methods

Animals

All animal procedures were performed in accordance with the Princeton University Institutional Animal Care and Use Committee regulations, and conformed to the National Research Council Guide for the Care and Use of Laboratory Animals (2011). Adult male and female C57BL/6J (catalog #000664) mice aged 12 weeks were obtained from The Jackson Laboratory. Upon arrival, all mice were group-housed in Optimice plastic cages on a reverse 12 h light/dark cycle, controlled for temperature and humidity with food and water available *ad libitum*. Mice were acclimated to the housing for 2 weeks before being bred in-house. For breeding, a single male and 2 females were group-housed in Optimice cages with bedding, paper nestlet and house. Pregnant females were individually housed and observed daily for parturition, deemed as postnatal day (PD) 0.

Maternal Separation with Early Weaning

C57BL/6J litters were pooled and 6-9 pups were distributed to each dam on PND2. These mice were then exposed to one of two conditions as previously described (1): 1) non-handled controls; or 2) handling with maternal separation for 4h daily from P2-P5 and 8h daily from P6-P16. The separation protocol was performed in the morning beginning between 09:00 and 10:00. Each dam was removed from the home cage to an adjacent cage with ad libitum access to food and water, and each litter was left in its home cage, which was placed on top of a thermal heating blanket maintained at 34°C. Pups remained with littermates for the entire period of separation after which they were reunited with the dam. MSEW pups were weaned at P17 while control litters were weaned normally at P21. Following weaning, all mice were group-housed in same sex, same litter groups until the start of behavioral testing at P60-P70. Body weight measurements were taken across different ages during development for MSEW mice, while control mice body weights were taken on the day of weaning. There were no postpartum deaths observed in the MSEW or control

groups. A total of 49 male mice (n=32; cohort 1, n=17; cohort 2) from 20 litters were behaviorally tested and data were analyzed as described in detail below.

Behavior

Anxiety testing

Mice were placed on an elevated plus maze (44 × 44 × 20 inches). Two of the arms had high walls (13 inches), whereas the other two arms and central intersection were open. All arms were 20 inches in length, with the open arms illuminated to 200 lux. Exploratory behavior was measured for 5 min and analyzed. The video was handscored by an experimenter measuring the number of entries and time spent in each of the open/closed arms for each mouse. Because the open arms are more exposed to the light and open air, more time spent in the open arms is considered a measure of reduced anxiety. Total entries into both closed and open arms are considered a measure of locomotion (2).

Activity testing

Mice were placed in the center of square acrylic open field (17.5 inches x 17.5 inches) with opaque walls and center illumination (300 lux). A camera was suspended 4 ft above the middle of the arena and each mouse was video recorded during the exploration period. Videos were analyzed with the BioViewer software and total distance travelled in the open field was used to assess activity and locomotion. Additionally, the amount of time mice spent active (movement above a preset velocity threshold of 1cm/s) was calculated as a percentage of the total time spent during the task. The speed of mice during the behavioral task was also calculated by the software.

Histochemistry

Subsets of mice from cohort 1 were perfused at age P60-P70, 2 hours after behavioral analyses. The 2 hour time point was selected because it is the time of maximal expression of immediate early gene protein product in inhibitory interneurons (3). Mice were deeply anesthetized with Euthasol and transcardially perfused with 4% paraformaldehyde (PFA) in PBS. Following perfusions, brains were postfixed for 48 h in 4% PFA, followed by cryoprotection with sucrose for 48h. 40μm-thick coronal sections were cut from half brains using a Cryostat (Leica Biosystems).

For immature neuron immunolabeling, free-floating sections obtained from a 1:6 series throughout the hippocampus were rinsed in phosphate-buffered saline (PBS) and then incubated

with 0.3% Triton X-100, 3% normal donkey serum, and goat anti-doublecortin in PBS at 4°C for 48 h. Sections were then washed and incubated with Alexa Fluor donkey anti-goat 568 for 1 h at room temperature.

For interneuron markers, Ki67 or OTX2 immunolabeling, free-floating sections that were rinsed in PBS were incubated with 3% normal donkey serum, PBS with 0.3% Triton X-100, and rabbit anti-calretinin, mouse anti-parvalbumin, rat anti- somatostatin, rabbit anti-Ki67 or anti-OTX2. All tissue was incubated in primary antisera for 48 h at 4°C, and then rinsed and incubated with secondary antisera, consisting of either Alexa Fluor donkey anti-mouse 488, Alexa Fluor donkey anti-rabbit 568 or Alexa Fluor donkey anti-rat 568. For GAD67 staining, sections first underwent antigen retrieval with 10mM sodium citrate buffer for 30min at 80°C, followed by incubation with mouse anti-GAD67 for 72 hours. Sections were then incubated in a biotinylated anti-mouse secondary with 10% normal horse serum for 1.5 hours using the Vectastain Elite ABC HRP-kit (Vector Laboratories). Following this, a metal enhanced DAB substrate kit (Thermo Fisher) was used to uncover GAD67 staining with high sensitivity in the hippocampal sections.

For WFA staining, sections were incubated in biotinylated Wisteria Floribunda Agglutinin (WFA) (1:500; Sigma), a plant-based lectin that labels N-acetylgalactosamine, a component of perineuronal nets (PNNs), for 48 hours at 4°C. After rinsing, the sections were incubated in streptavidin 488 (1:500). Sections were rinsed, mounted onto Suprafrost slides, and cover-slipped using glycerol in PBS (3:1). Antibody species and dilution are detailed in Supplemental Table S1.

Cell Count and Density Analyses

All slides were coded until completion of the data analysis. Whole cell counts of DCX and Ki67 were made in the granule cell layer (GCL) of the hippocampus and interneuron subtypes were counted across all layers of the hippocampal subfields using the Stereo Investigator software (Microbrightfield Bioscience). Briefly, the extent of the individual subregions (polymorphic layer (PO), granule cell layer (GCL), molecular layer (MOL), stratum lacunosum-moleculare (LAC), stratum radiatum (RAD), stratum pyramidale (PYR), and stratum oriens (OR)) were outlined, and labeled cells within the delineated region were counted. Densities were determined by dividing the total number of positive cells by the volume of the region outlined.

WFA and OTX2 Analyses

All brains were processed together in exactly the same manner after perfusion 2 hours after the last behavioral task. Brain tissue was cut in 40μm sections on the cryostat. Ventral sections from a 1:6 series of each brain were triple labelled with WFA, OTX2 and PV in a single reaction to control for potential variation in staining and tissue processing. Images of labeled cells from all brains were acquired in parallel on the confocal microscope (Zeiss-LSM700) with the 20X objective, within the same time period in stacks of 2μm through the entire section. Image analysis was adapted from a previously published protocol (4). Images from all brains were taken with identical confocal settings to allow for cross comparisons of intensities between groups. ImageJ (NIH) was used to analyze all image z-stacks. First, the rolling ball radius function was used to remove background staining on all image stacks. Next, the maximum intensity projection was used as a reference to identify all PV cells and PNNs. A region of interest (ROI) was created by tracing every PV+/WFA+ cell in the image with the tracing tool, and the area and intensity (mean gray value of WFA or OTX2 x area of the WFA stain) for each WFA+/PV+ cell were determined at each plane throughout the z stack. The plane of maximum intensity for WFA or OTX2 was then used to calculate and record the intensities of WFA or OTX2 for all cells in control and MSEW groups. WFA intensity values from both groups were plotted in a histogram and fitted with a Gaussian curve to determine whether there was a shift in the number of cells falling into each intensity bin. Analyses of WFA and PV cell counts and percentage colocalization were conducted in a similar manner to the cell counts described earlier.

PV Intensity Analysis

Similar to the WFA analysis detailed above, ventral hippocampus sections from a 1:6 series of 16 control and MSEW brains were stained for PV in a single immunohistochemistry reaction. This analysis was a modified version of a previously published protocol (5). High magnification images of the PV soma at its maximum plane of intensity were acquired in 1μm stacks on the confocal microscope (Zeiss-LSM700) with identical confocal settings using a x63/1.4 oil immersion objective. Image J was used to analyze all images. Images from all brains were taken with identical confocal settings to allow for cross comparisons of intensities between groups. The rolling ball radius function was used to remove background staining on all image stacks. The soma of the PV

cell was marked as the ROI with the tracing tool and the intensities and areas of all PV cells in the sections was recorded.

Surgery

Mice were deeply anesthetized with isoflurane (2-3%), shaved and placed in a stereotaxic instrument (David Kopf Instruments) under a temperature controlled thermal blanket. Anterior-posterior and medial-lateral coordinates were measured from bregma, while depth was calculated relative to the brain surface. Insulated stainless steel electrodes (0.005", Plastics One) were implanted through burr holes targeting the vHIP CA1; (3.3 mm posterior, 3.45 mm lateral and 4.2 mm depth). Two bone screws (FST) were implanted on the contralateral posterior portion of the skull and the contralateral mPFC and one screw was used as a ground. A separate bare stainless steel ground wire was wrapped around the ground screw over the contralateral mPFC. A base layer of MetaBond (Parkell) was applied to the skull and implant, and allowed to dry before dental acrylic (Bosworth) was used to build up the skull cap. Following surgery, mice were given a week to recover before habituation and behavior experiments.

LFP Recordings and Analysis

One week after surgery, mice were familiarized to the recording setup and handling by being tethered to the headstage preamplifier in their home cages for three sessions daily of 15 min each. On the third day, mice were exposed to an empty cage (familiar environment) for 2 sessions of 15 min each. LFP recording data were collected on the fourth day from two separate recording sessions. First, mice were exposed to the familiar environment for a period of 10 min followed by an hour of rest and then exposed to a novel environment for a period of 10 min. The novel environment consisted of an acrylic box (17 cm x 17 cm x 17 cm) illuminated to approximately 200 lux by a lamp hanging directly overhead. LFPs were recorded against a ground screw placed above the mPFC. Signals were passed through a commutator, amplified 100X, and sampled at 1000 Hz using a Cambridge Electronic Design 1401 data acquisition unit and Spike2 software. Signals were notch filtered at 60 Hz and artifacts related to movement, detected using a voltage threshold, were removed from the data. Power spectra were calculated from data acquired from mice during segments of movement only (4-15 cm/s). Animals with less than 5 seconds of data during movement were excluded from analysis. Power spectral density was estimated using short-

time Fourier transform. To obtain power estimates within theta and gamma bands, the average power across time for the entire session within each frequency was taken, followed by the sum of this average power across the entire frequency band. To examine changes in theta and gamma power between groups, Mann Whitney U tests were performed on the sum of power within the theta and gamma bands. For phase amplitude coupling analyses, all mice, regardless of movement (moving or stationary) were included in the analysis. Theta (4-12 Hz) and gamma (30-80 Hz) signals were filtered separately using a band-pass Butterworth filter, and analytic signals were obtained using the Hilbert transformation. Instantaneous theta phase was measured as the angle of the analytic theta signal, and instantaneous gamma amplitude was measured as the absolute value of the magnitude of the analytic gamma signal. To calculate the modulation index, average gamma amplitude within theta frequency bins (each bin 3.6 degrees) was measured, and the difference between the maximum gamma amplitude and minimum gamma amplitude as a function of theta frequency was calculated (6).

Statistical Tests

One animal was identified as a statistical outlier on the Grubbs' test and was excluded from the activity test data. Either unpaired two tailed Student's t-tests or Mann-Whitney tests were performed on all data sets following determination of homogeneity of variance with Levene's test.

Supplemental Discussion

Reliability and Translational Validity of Animal Models of Early Life Adversity

Numerous studies have pointed to a link between early life adversity and an increased incidence of neuropsychiatric disorders in adulthood (7-9). Most of these studies have shown that the type of adversity experienced during childhood (physical or emotional abuse, or physical or emotional neglect) is a less important factor in determining mental health outcomes than how much adversity was experienced overall (10; 11). Several reports, including a recent large study, have shown that the cumulative effects of adverse events are most predictive of increased incidence of mental illness (11). Given this strong association between early life stress and mental illness, it is not surprising that many groups have attempted to model this relationship in animals in an effort to better explore its biological underpinnings. Unfortunately, however, while there is little

contradiction in the human literature on this subject of whether there is a connection between early life stress and mental health difficulties in later life, the animal literature is rife with discrepant findings. As discussed in our recent commentary (12) some of these contradictory findings may be the result of individual differences in vulnerability versus resilience to early life adversity. Thus, in cases where comparisons are made across groups, small studies may result in null effects because they are underpowered, unlike most human studies which tend to include larger numbers of subjects. For these reasons, we included a large number of animals in our studies and verified the expected behavioral outcome (increased anxiety-like behavior) in two different cohorts. In addition, maternal separation with early weaning is an animal model that specifically produces two behavioral changes similar to human disorders that have been strongly associated with early life adversity; excessive anxiety and ADHD. Early weaning by itself has been shown to result in increased anxiety in both mice and rats (13; 14) and the combination of early weaning with maternal separation in this model also results in increased hyperactivity, which is of particular relevance as reports have shown a link between ADHD and childhood trauma/abuse (11; 15; 16). Furthermore, ADHD and anxiety disorders exhibit 50% comorbidity (17). Our experience and findings strongly suggest that MSEW is a valid animal model of early life adversity increasing anxiety and hyperactivity in humans, as it represents a model of cumulative adversity during childhood and reliably produces the expected behavioral outcome.

Cell Autonomous OTX2 and Stress Resilience

OTX2 is a transcription factor that is prevalent in the fetal brain, where it works in both cell and non-cell autonomous ways to direct brain organization, cell proliferation and neural fate (18-20). In the adult brain, the expression of OTX2 is much more restricted and is localized primarily to the choroid plexus and the dopaminergic neurons of the ventral tegmental area (VTA) (20; 21). Similar to development, OTX2 in adulthood can exert its actions through both cell and non-cell autonomous pathways. The involvement of OTX2 in visual cortex plasticity is known to be non-cell autonomous, with OTX2 originating from the choroid plexus sequestered by PV+ cells in the occipital cortex where it works to maintain PNNs (18). Our data suggest that OTX2 may work through a similar mechanism to regulate early life stress-induced changes in adult PNN expression in that MSEW increases OTX2 expression in the choroid plexus, where it is known to be synthesized. MSEW also increases OTX2 protein labeling in PV+/PNN+ cells of the vHIP, a brain

region which does not contain OTX2 mRNA (18), suggesting that the protein must be made elsewhere, most likely in the choroid plexus, where it enters the CSF and is ultimately taken up by PV+ PNN+ cells. The increase in OTX2 and PNNs surrounding PV+ cells, which are known to generate theta rhythm associated with increased anxiety, suggests that OTX2 may play a role in early life stress-induced increases in anxiety. By contrast, OTX2 seems to be play a cell autonomous role in the adult VTA where its absence after early life stress confers vulnerability to adult stress-induced depressive-like symptoms (22). In this system, OTX2 is made by dopaminergic neurons in the VTA and early life stress diminishes its expression. Restoration of OTX2 levels in this system prevents stress-induced vulnerability in later life. Although at face value these findings seem to show that OTX2 has opposite responses to stress in the different brain regions, as well as opposite functional outcomes, the mechanisms differ considerably in that unlike in the VTA, OTX2 in the vHIP is not made by the neurons which it influences (18). Furthermore, it is worth noting that manipulating OTX2 in the VTA had no effect on anxiety-like behaviors in the previous study (22), raising another important difference between that study and ours. It may be the case that like many other molecules in the brain, OTX2 has multiple modes of action, as well as multiple functions.

Supplemental Figures and Tables

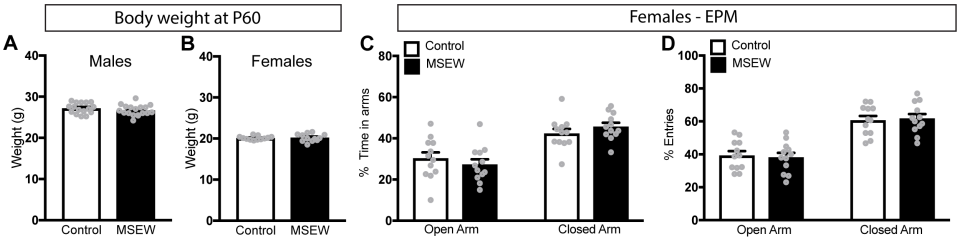

Fig S1: MSEW does not affect body weight at adulthood in either male (A) or female mice (B). (C-D) Female mice do not show anxiety-like behaviors in the EPM.

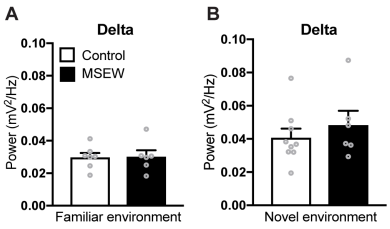

Fig S2: Delta power in ventral hippocampus of control and MSEW mice is not altered in the (A) familiar environment or (B) novel environment.

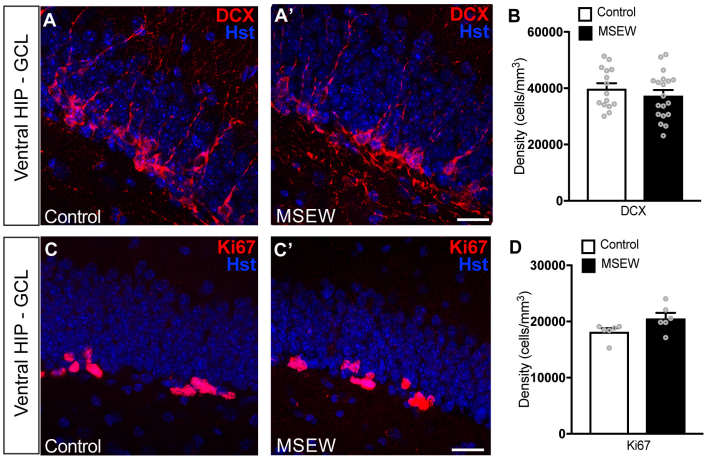

Fig S3: (A,A') DCX expression in the ventral hippocampus GCL of control and MSEW mice. (B) Graph showing no difference in DCX densities between groups. (C-C') Ki67 expression in the ventral hippocampus GCL of control and MSEW mice. (D) Graph showing no difference in Ki67 densities between groups in ventral hippocampus.

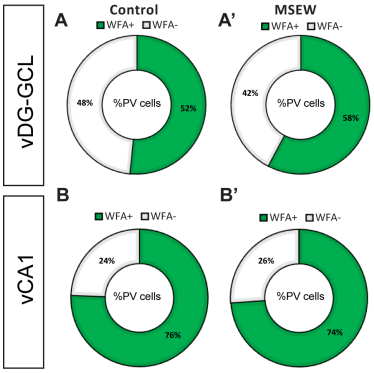

Fig S4: Graphs showing no differences in the percentage of PV+ interneurons expressing WFA in the ventral hippocampus GCL (A-A') and CA1 (B-B') of control and MSEW mice.

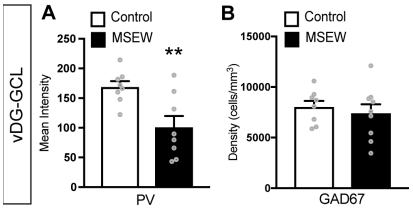

Fig S5: (A) Graph showing that the intensity of PV staining in PV+ interneurons in the ventral hippocampus GCL is significantly lower in MSEW animals compared to controls. (B) Graph showing that the density of cells stained with the pan interneuron marker GAD67+ in the ventral hippocampus GCL is unaltered between control and MSEW mice.

Table S1: Antibody Table

Name	Species	Dilution	Type	Company
Doublecortin (DCX)	goat	1:100	Primary	Santa Cruz Biotechnology
Ki67	rabbit	1:100	Primary	Abcam
Parvalbumin (PV)	mouse	1:500	Primary	Swant
Calretinin (CR)	rabbit	1:500	Primary	Swant
Somatostatin (SST)	rat	1:200	Primary	Millipore
C-fos	rabbit	1:500	Primary	Cell Signaling Technology
GAD67	mouse	1:250	Primary	Millipore
Othrodenticle Homeobox Protein 2 (OTX2)	rabbit	1:500	Primary	Protein Tech
Alexa Fluor anti-goat 568	donkey	1:500	Secondary	Invitrogen
Alexa Fluor anti-mouse 488	donkey	1:500	Secondary	Invitrogen
Alexa Fluor anti-rabbit 568	donkey	1:500	Secondary	Invitrogen
Alexa Fluor anti-rabbit 488	donkey	1:500	Secondary	Invitrogen
Alexa Fluor anti-rat 568	donkey	1:500	Secondary	Invitrogen

Table S2: Statistics table

Behavior

Cohort	Behavioral Paradigm	Measurement	Statistical Test	Comparison	t / U value	° of freedom (df)	p value	*	Fig.
1	Elevated Plus Maze (EPM)	% entries into open arms	t-test	Control vs MSEW	2.554	30	0.016	*	1B
1	Elevated Plus Maze (EPM)	% entries into closed arms	t-test	Control vs MSEW	2.554	30	0.016	*	1B
1	Elevated Plus Maze (EPM)	% time in open arms	t-test	Control vs MSEW	2.006	30	0.054	-	1C
1	Elevated Plus Maze (EPM)	% time in closed arms	t-test	Control vs MSEW	2.148	30	0.039	*	1C
2	Elevated Plus Maze (EPM)	% entries into open arms	t-test	Control vs MSEW	2.839	15	0.012	*	1D
2	Elevated Plus Maze (EPM)	% entries into closed arms	t-test	Control vs MSEW	2.839	15	0.012	*	1D
2	Elevated Plus Maze (EPM)	% time in open arms	Mann-Whitney	Control vs MSEW	*U*=28	-	0.481	-	1E
2	Elevated Plus Maze (EPM)	% time in closed arms	t-test	Control vs MSEW	0.071	15	0.945	-	1E
1	Activity test (Open Field)	Total distance travelled (cm)	t-test	Control vs MSEW	2.514	29	0.018	*	2A
1	Activity test (Open Field)	%Activity	t-test	Control vs MSEW	2.659	29	0.013	*	2B
1	Activity test (Open Field)	Speed in box	t-test	Control vs MSEW	2.514	29	0.018	*	2C

Electrophysiology

Cohort	LFP data	Environment	Measurement	Statistical Test	Comparison	t / U value	° of freedom (df)	p value	*	Fig.
2	LFP band power	Familiar	Theta	t-test	Control vs MSEW	0.957	12	0.358	-	3D
2	LFP band power	Familiar	Alpha/beta	Mann Whitney	Control vs MSEW	*U=19*	-	0.535	-	3E
2	LFP band power	Familiar	Gamma	Mann-Whitney	Control vs MSEW	*U*=19	-	0.535	-	3F
2	LFP band power	Novel	Theta	Mann-Whitney	Control vs MSEW	*U*=6	-	0.012	*	3K
2	LFP band power	Novel	Alpha/beta	t-test	Control vs MSEW	2.323	13	0.037	*	3L
2	LFP band power	Novel	Gamma	Mann Whitney	Control vs MSEW	*U=24*	-	0.776	-	3M
2	Phase amplitude coupling	Familiar	Modulation Index	t-test	Control vs MSEW	2.424	13	0.0307	*	3H
2	Phase amplitude coupling	Novel	Modulation Index	t-test	Control vs MSEW	2.627	14	0.0199	*	3O

Cell density

Cohort	Measurement	Region	Cell subtype	Statistical Test	Comparison	t / U value	° of freedom (df)	p value	*	Fig.
1	Cell density	vDG	PV	t-test	Control vs MSEW	2.323	17	0.033	*	4B
1		vCA1	PV	Mann-Whitney	Control vs MSEW	*U*=23	-	0.270	-	4B’
1		vCA3	PV	t-test	Control vs MSEW	0.700	15	0.495	-	4B’’
1		vDG	SST	t-test	Control vs MSEW	3.244	10	0.009	*	4D
1		vCA1	SST	t-test	Control vs MSEW	0.237	10	0.828	-	4D’
1		vCA3	SST	t-test	Control vs MSEW	0.162	10	0.874	-	4D’’
1		vDG	CR	t-test	Control vs MSEW	1.26	10	0.236	-	4F
1		vCA1	CR	t-test	Control vs MSEW	0.743	10	0.475	-	4F’
1		vCA3	CR	t-test	Control vs MSEW	1.556	10	0.151	-	4F’’
1		vDG	PV/c-fos	t-test	Control vs MSEW	0.354	10	0.731	-	4H
1		vCA1	PV/c-fos	t-test	Control vs MSEW	0.755	10	0.468	-	4H’
1		vDG	SST/c-fos	t-test	Control vs MSEW	0.751	10	0.470	-	4J
		vCA1	SST/c-fos	t-test	Control vs MSEW	0.588	10	0.570	-	4J’
1		vDG	WFA	t-test	Control vs MSEW	0.939	10	0.370	-	5D
1		vCA1	WFA	t-test	Control vs MSEW	0.106	10	0.918	-	5F

Staining intensity

Cohort	Measurement	Region	Cell subtype	Statistical Test	Comparison	t / U value	° of freedom (df)	p value	*	Fig.
1	Staining intensity	vDG-GCL	Low WFA	t-test	Control vs MSEW	7.228	10	<0.0001	***	5C
1		vDG-GCL	High WFA	t-test	Control vs MSEW	2.467	10	0.033	-	5C
1		vCA1	Low WFA	t-test	Control vs MSEW	0.437	10	0.672	-	5E
1		vCA1	High WFA	t-test	Control vs MSEW	1.14	10	0.281	-	5E
1		Choroid plexus	Otx2	Mann-Whitney	Control vs MSEW	*U*=23	-	0.047	*	6B
1		vDG-GCL	PV+/WFA+	t-test	Control vs MSEW	2.471	14	0.027	*	6D
1		vDG-GCL	PV+/WFA-	t-test	Control vs MSEW	1.695	13	0.114	-	6E

Table S3: Supplemental figure statistics table

Cohort	Test	Measurement	Type/Region	Statistical Test	Comparison	t / U value	° of freedom (df)	p value	*	Fig.
1	Body weight data	Weight	Males	t-test	Control vs MSEW	1.176	32	0.248	-	S1A
1	Body weight data	Weight	Females	t-test	Control vs MSEW	0.306	22	0.763	-	S1B
2	Elevated Plus Maze (EPM)	% entries into open arms	Females	t-test	Control vs MSEW	0.295	22	0.771	-	S1C
2	Elevated Plus Maze (EPM)	% entries into closed arms	Females	t-test	Control vs MSEW	0.295	22	0.771	-	S1C
2	Elevated Plus Maze (EPM)	% time in open arms	Females	t-test	Control vs MSEW	0.774	22	0.447	-	S1D
2	Elevated Plus Maze (EPM)	% time in closed arms	Females	t-test	Control vs MSEW	1.166	22	0.256	-	S1D
2	LFP band power	Delta power	Familiar	t-test	Control vs MSEW	0.024	12	0.981	-	S2A
2	LFP band power	Delta power	Novel	t-test	Control vs MSEW	0.230	13	0.822	-	S2B
1	Cell density	DCX	vDG-GCL	t-test	Control vs MSEW	0.907	32	0.371	-	S3B
1	Cell density	Ki67	vDG-GCL	t-test	Control vs MSEW	2.114	10	0.061	-	S3D
1	% cell colocalization	% PV that are WFA+	vDG-GCL	t-test	Control vs MSEW	1.07	10	0.312	-	S4A-A’
1	% cell colocalization	% PV that are WFA+	vCA1	t-test	Control vs MSEW	0.373	10	0.717	-	S4B-B’
1	staining intensity	PV+ Cell intensity	vDG-GCL	t-test	Control vs MSEW	3.183	14	0.007	**	S5
1	Cell density	GAD67	vDG-GCL	t-test	Control vs MSEW	0.579	15	0.571	-	S5

Supplemental References

1. George ED, Bordner KA, Elwafi HM, Simen AA (2010) Maternal separation with early weaning: a novel mouse model of early life neglect. *BMC Neurosci*. 11:123.
2. File SE, Aranko K (1988) Sodium valproate and chlordiazepoxide in the elevated plus-maze test of anxiety in the rat. *Neuropsychobiology*. 20:82-86.
3. Peng Z, Houser CR (2005) Temporal patterns of fos expression in the dentate gyrus after spontaneous seizures in a mouse model of temporal lobe epilepsy. *J Neurosci*. 25:7210-7220.
4. Slaker ML, Harkness JH, Sorg BA (2016) A standardized and automated method of perineuronal net analysis using Wisteria floribunda agglutinin staining intensity *IBRO Rep*. 1:54-60.
5. Donato F, Rompani SB, Caroni P (2013) Parvalbumin-expressing basket-cell network plasticity induced by experience regulates adult learning Nature 504:272-276.
6. Tort AB, Komorowski R, Eichenbaum H, Kopell N (2010) Measuring phase-amplitude coupling between neuronal oscillations of different frequencies. *J Neurophysiol*. 104:1195-1210.
7. Heim C, Shugart M, Craighead WE, Nemeroff CB (2010) Neurobiological and psychiatric consequences of child abuse and neglect. *Dev Psychobiol*. 52:671-690.
8. Schalinski I, Breinlinger S, Hirt V, Teicher MH, Odenwald M, Rockstroh B (2017) Environmental adversities and psychotic symptoms: The impact of timing of trauma, abuse, and neglect. *Schizophr Res*. pii: S0920-9964(17)30662-X
9. Gallo EAG, Munhoz TN, Loret de Mola C, Murray J (2018) Gender differences in the effects of childhood maltreatment on adult depression and anxiety: A systematic review and meta-analysis. *Child Abuse Negl*. 79:107-114.
10. Dunn EC, Soare TW, Raffeld MR, Busso DS, Crawford KM, Davis KA, et al. (2018) What life course theoretical models best explain the relationship between exposure to childhood adversity and psychopathology symptoms: recency, accumulation, or sensitive periods? *Psychol Med*.1-11.
11. Copeland WE, Shanahan L, Hinesley J, Chan R, Aberg KA, Fairbank JA, et al (2018) Association of childhood trauma exposure with adult psychiatric disorders and functional outcomes. *JAMA Netw Open.* 1:e184493.
12. Murthy S, Gould E (2018) Early life stress in rodents: animal models of illness or resilience? *Front Behav Neurosci*. 12:157.
13. Kikusui T, Takeuchi Y, Mori Y (2004) Early weaning induces anxiety and aggression in adult mice. *Physiol Behav*. 81:37-42.
14. Ito A, Kikusui T, Takeuchi Y, Mori Y (2006) Effects of early weaning on anxiety and autonomic responses to stress in rats. *Behav Brain Res*. 171:87-93.
15. Fuller-Thomson E, Mehta R, Valeo A (2014) Establishing a link between attention deficit disorder/attention deficit hyperactivity disorder and childhood physical abuse. *J Aggress Maltreat T*. 23:188-198.
16. Bjorkenstam E, Burstrom B, Vinnerljung B, Kosidou K (2016) Childhood adversity and psychiatric disorder in young adulthood: An analysis of 107,704 Swedes. *J Psychiatr Res*. 77:67-75.

17. Mao AR, Findling RL (2014) Comorbidities in adult attention-deficit/hyperactivity disorder: a practical guide to diagnosis in primary care. *Postgrad Med*. 126:42-51.
18. Spatazza J, Lee HH, Di Nardo AA, Tibaldi L, Joliot A, Hensch TK, et al. (2013) Choroid plexus-derived OTX2 homeoprotein constrains adult cortical plasticity. *Cell Rep*. 3:1815-1823.
19. Spatazza J1, Di Lullo E, Joliot A, Dupont E, Moya KL, Prochiantz A (2013) Homeoprotein signaling in development, health, and disease: a shaking of dogmas offers challenges and promises from bench to bed. *Pharmacol Rev* 65:90-104.
20. Sugiyama S, Prochiantz A, Hensch TK (2009) From brain formation to plasticity: insights on Otx2 homeoprotein. *Dev Growth Differ*. 51:369-377.
21. Panman L, Papathanou M, Laguna A, Oosterveen T, Volakakis N, Acampora D et al. (2014) Sox6 and Otx2 control the specification of substantia nigra and ventral tegmental area dopamine neurons. *Cell Rep* 8:1018-1025.
22. Peña CJ, Kronman HG, Walker DM, Cates HM, Bagot RC, Purushothaman I et al. (2017) Early life stress confers lifelong stress susceptibility in mice via ventral tegmental area OTX2. *Science* 356:1185-1188.